**Supplementary Information**

# Ultrafast synthesis and switching of light polarization in nonlinear anisotropic metamaterials

Luke H. Nicholls[1], Francisco J. Rodríguez-Fortuño[1], Mazhar E. Nasir[1], R. Margoth Córdova-Castro[1], Nicolas Olivier[1]†, Gregory A. Wurtz[1]‡, Anatoly V. Zayats[1]

[1]Department of Physics, King's College London, Strand, London WC2R 2LS, UK

†Present address: Department of Physics, The University of Sheffield, Sheffield, S10 2TN, UK

‡Present address: Department of Physics, University of North Florida, Jacksonville Florida 32224, USA

## Material fabrication

The studied nanorod metamaterials were fabricated using an electrochemical approach and comprise of Au nanorod arrays in alumina matrix. Electrochemical fabrication provides metamaterial samples over macroscopic, in this case centimeter square size, areas. The metamaterial's permittivity tensor can be tailored during fabrication by tuning the geometric parameters of the nanorod arrays[28,29]. The porous alumina matrix was synthesized by a two step-anodization of an Al film. The Al film was deposited by magnetron sputtering on a substrate comprising of a 1 mm thick glass slide with a 10 nm thick adhesive layer of tantalum pentoxide, and an approximately 5 nm thick Au film acting as a weakly conducting electrode. The period and diameter of nanopores can be designed by carefully controlling the anodization conditions (choice of acid, anodization temperature and voltage). Accounting for volume expansion on anodization of the Al film, a 400 nm thick porous alumina template is formed. Gold electrodeposition was performed with a three-electrode system using a non-cyanide solution. The length of the nanorods was controlled by the electrodeposition time.

Two different metamaterials were investigated: one with nanorod array parameters 400 nm length, 70 nm period, and 30 nm diameter with the effective plasma frequency at approximately 720 nm and another with parameters 210 nm length, 120 nm period, 70 nm diameter with the effective plasma frequency at approximately 590 nm.

**Optical Measurements**

The modulation of polarization state of transmitted light through the metamaterial was measured by polarization resolved pump-probe spectroscopy. The system utilizes two outputs from an amplified Ti-sapphire femtosecond laser system (Supplementary Fig. 5). The first output is sent to an optical parametric amplifier tunable in a wavelength range of 500 to 750 nm used as a control beam. The second output (800 nm wavelength) is sent through a sapphire plate to generate a white light continuum used as signal light to probe the optical properties of the sample. The probe is delayed in time with respect to the pump by an optical delay line. A system of half and quarter waveplates is used to optimize a diagonal polarization of the signal at the detector after the sample. Measurements are then taken at different delay times to determine the transmission intensity changes for co- and cross-polarized (with respect to ground state polarization) light as well as for both ordinary and extraordinary waves (Fig. 2a,b). These four transient transmission measurements are then used to recover the polarization ellipse of the transmitted light at each delay time through least squares fits (Fig. 3a) from which the rotation angles can be obtained (Fig. 3b,c).

**Numerical Modelling**

Numerical simulations where performed using the frequency domain method in the commercial software CST Microwave Studio. A unit cell was simulated including a single

rod. Floquet modes with different polarizations were considered for excitation and analysis, with an incident angle of $\theta = 45^{o}$ in air. The gold rods where considered ideal cylinders with radius 14.5 nm, height 425 nm and periodicity 71 nm. The rods were embedded in an alumina matrix with refractive index 1.76 of the same height as that of the rods. The rods were simulated on top of a 15 nm thin layer of gold, and a 5 nm thin layer of tantalum pentoxide with refractive index 2.1. A semi-infinite glass substrate was used with refractive index 1.44. These refractive indices were considered constant in the simulated wavelength range, while the permittivity of gold was defined with the dispersive model described below, which allows also to include the effect of the control light which leads to changes in electron temperature of Au.

Transmission coefficients for both ordinary and extraordinary waves were simulated in both ground ($T_e$ = 300 K) and excited ($T_e$ > 300 K) states. Knowing the two complex TE and TM Fresnel transmission coefficients and using Eq. 1, we analytically obtain the output polarization for any desired input polarization, or conversely, obtain the required input polarization for a desired output polarization.

The nonlinear permittivity of Au was modeled within the random phase approximation where the energy deposited in the electron population by the control (pump) beam is described by an equilibrium temperature $T_e$ determined by a Fermi-Dirac energy distribution[9]. Both inter- and intra-band transitions contribute to the nonlinear permittivity as $\varepsilon_{\mathrm{Au}} = \varepsilon_{\mathrm{inter}} + \varepsilon_{\mathrm{intra}}$, where the intraband term, describing the response of s-band electrons, is of a Drude form

$$\varepsilon_{\mathrm{intra}} = 1 - \frac{\omega_{\mathrm{p}}}{\omega(\omega + i\gamma_{\mathrm{intra}}(\omega, T_{\mathrm{e}}, T_{\mathrm{L}})}, \qquad (1)$$

with a plasma frequency $\omega_{\mathrm{p}}$ = 2.168×10$^{15}$ s$^{-1}$ and an electron-electron and electron-phonon scattering-dependent damping term $\gamma_{\mathrm{intra}}$ [9]; and interband contributions from electrons in the d-band take a Lorentzian lineshape of the form

$$\varepsilon_{\mathrm{inter}} = K\int_0^{\infty} dx \frac{\sqrt{\hbar x - E_{\mathrm{g}}}}{x}\left(1 - f(x, T_e)\right) \cdot \frac{\left(\gamma_{\mathrm{inter}}(\omega,T_{\mathrm{e}},T_{\mathrm{L}})^2 - \omega^2 + x^2\right) + 2i\omega\gamma_{\mathrm{inter}}(\omega,T_{\mathrm{e}},T_{\mathrm{L}})}{\left(\gamma_{\mathrm{inter}}(\omega,T_{\mathrm{e}},T_{\mathrm{L}})^2 - \omega^2 + x^2\right) + 4\gamma_{\mathrm{inter}}(\omega,T_{\mathrm{e}},T_{\mathrm{L}})^2\omega^2} \qquad (2)$$

where $E_{\mathrm{g}}$ = 1.98 eV is the energy of the bandgap between a dispersionless *d*-band and a parabolic *sp* band, $K$ = 1.2695×10$^{32}$ represents the strength of the interband transition dipole moment, $\gamma_{\mathrm{inter}}$ is the associated scattering damping term and $f(x, T_{\mathrm{e}})$ is the Fermi-Dirac distribution of electrons at the temperature $T_{\mathrm{e}}$. Furthermore, in order to more closely model the permittivity of electrodeposited gold[30], the electron mean free path is reduced from that of bulk gold ($L$ = 35.7 nm) to a restricted value ($R$ = 10 nm). This gives a corrected permittivity

$$\varepsilon_{\mathrm{c}} = \varepsilon_{\mathrm{Au}} + \frac{i\omega_{\mathrm{p}}^2\tau(L-R)}{\omega(\omega\tau+i)(\omega\tau R+iL)}. \qquad (3)$$

This term is then calculated at different values of $T_{\mathrm{e}}$ and used in the CST model to simulate the excited state.

**Effective medium description of the metamaterials**

The effective permittivity tensor of a nanorod metamaterial can be expressed in terms of principal components within the effective medium theory[31] as $\varepsilon_{\mathrm{eff}} = \mathrm{diag}\left(\varepsilon_x, \varepsilon_y = \varepsilon_x, \varepsilon_z\right)$, where the frequency-dependence is implicit and the Cartesian co-ordinate system is defined in Fig. 1a. The spectra of the permittivity components for the studied metamaterials are shown in Supplementary Fig. 1, which describes the measured optical response of the metamaterial sample. The anisotropic permittivity results in a metamaterial supporting two dispersion regimes, transitioning between an elliptic ($\varepsilon_x, \varepsilon_z > 0$) and an hyperbolic ($\varepsilon_x >$

$0, \varepsilon_z < 0$) dispersion at the effective plasma frequency $\omega_{\mathrm{p}}^{eff}$ corresponding to a free-space wavelength of approximately 725 nm (Supplementary Fig. 1), where $\mathrm{Re}(\varepsilon_z)$ experiences a change of sign[25]. Please note that a conventional "local" effective medium approximation may not be adequate under certain conditions when nonlocal (spatial dispersion effects) are important[32,33]. At the same time, numerical simulations taking into account the microscopic internal structure of a metamaterial can always be used.

As for conventional anisotropic materials, nanorod-based metamaterials support ordinary *o*-waves with polarization normal to the principal (*z*-) axis and refractive index $n_{\mathrm{o}} = (\varepsilon_x)^{\frac{1}{2}}$, as well as extraordinary *e*-waves, with a polarization component in the principal plane and refractive index dependent on the direction of propagation within the metamaterial $\frac{1}{n_e^2} = \frac{\cos^2\alpha}{\varepsilon_x} + \frac{\sin^2\alpha}{\varepsilon_z}$, where $\alpha$ defines the angle of propagation in the material with respect to the principal (*z*-) axis[24].

**Retrieval of polarization ellipse from four power measurements**

We retrieve the complex Jones' vector of output polarization from the values of measured intensity after a linear polarizer in four different orientations ($\theta_i = -45°, 0°, 45°, 90°$). The aim is to find the polarization Jones' vector $\mathbf{E} = (E_o, E_e)$, with both components complex in general. We can apply an arbitrary global phase which does not change the polarization, such that we may consider one of the components as being only real and positive, resulting in three unknown real quantities $\mathbf{E} = (E_o^{\mathrm{re}}, E_e^{\mathrm{re}} + iE_e^{\mathrm{im}})$.

The intensity measured after a linear polarizer is given by $P(\theta) \propto |\mathbf{E} \cdot \mathbf{u}(\theta)|^2$, where $\mathbf{u}(\theta)$ is a unit vector in the direction $\theta$ of the polarizer. We arbitrarily define $\theta$ such that $\mathbf{u}(\theta) = (\sin\theta\,, \cos\theta)$, so the squared dot product yields:

$$P(\theta) \propto \left(E_o^{\mathrm{re}\,2}\right) \sin^2\theta + 2\left(E_o^{\mathrm{re}} E_e^{\mathrm{re}}\right) \cos\theta \sin\theta + \left(E_e^{\mathrm{re}\,2} + E_e^{\mathrm{im}\,2}\right) \cos^2\theta$$

$$= A \sin^2\theta + 2B \cos\theta \sin\theta + C \cos^2\theta$$

From the four measurements $P(\theta_i)$, we can fit the three parameters A, B, and C, constituting an overdetermined linear system. We solve it using linear algebra corresponding to a least squared error fit. From these three parameters, we can retrieve the polarization components as $E_o^{\mathrm{re}} = \sqrt{A}$, $E_e^{\mathrm{re}} = B/\sqrt{A}$, and $E_e^{\mathrm{im}} = \pm\sqrt{C - B^2/A}$, where the sign of the square root represents the uncertainty on the polarization handedness.

In Supplementary Fig. 6, we show an example of polar plots of $P(\theta)$ for the retrieved polarization ellipses in Fig. 4, together with the four measured intensity data points. While three intensity measurements can always be fitted exactly with three parameters, the good fit achieved with four intensity measurements shows the robustness of the measurements and retrieval procedure.

**Supplementary Figures**

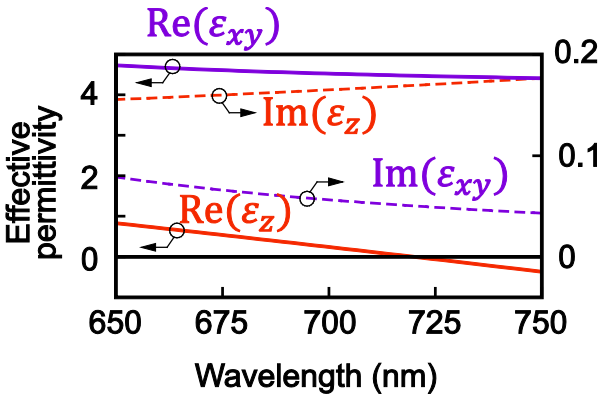


**Supplementary Figure 1. Effective permittivity tensor components of the metamaterial** with a nanorod diameter and a period of 30 nm and 70 nm, respectively. The permittivity spectra were obtained by fitting the measured spectra for different angles of incidence with the effective permittivity functional as in Ref. 3.

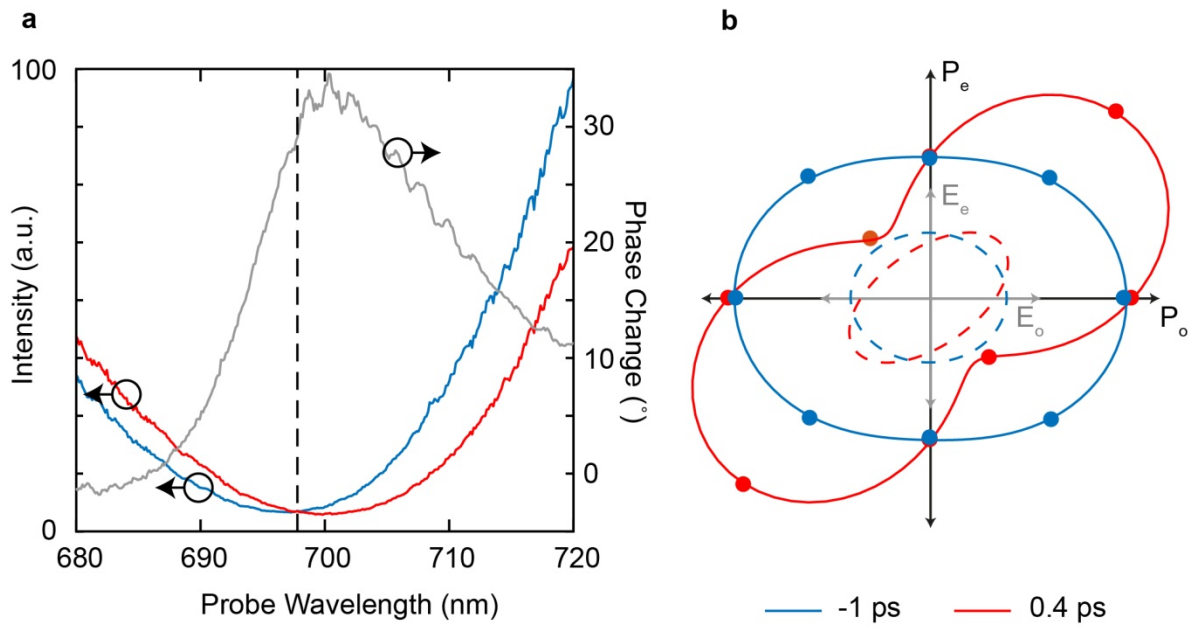


**Supplementary Figure 2. Transmitted intensity, phase and polarization variations on control light excitation. (a)** Spectra of the non-normalized measured intensity of the extraordinary polarization component of the signal light at time-delays $\Delta t = -1$ ps (blue) and $\Delta t = 0.4$ ps (red) with respect to the control light pulse arrival time. The grey dashed curve is the retrieved phase change of the extraordinary component of transmitted electric field, calculated as the difference in relative phase of ordinary and extraordinary waves $\Delta\varphi = \arg\left(\frac{E_e(\Delta t = -1\text{ ps})}{E_o(\Delta t = -1\text{ ps})}\right) - \arg\left(\frac{E_e(\Delta t = 0.4\text{ ps})}{E_o(\Delta t = 0.4\text{ ps})}\right)$, retrieved from polarization measurements. The phase of ordinary wave $E_o$ is assumed to be unchanged upon the excitation. **(b)** The intensity measurements at each analyser angle fitted at these two times, at a wavelength of 696.6 nm, at which both ordinary and extraordinary intensities have negligible variations, so the polarization change is caused by phase changes. The corresponding recovered polarization ellipses are plotted as an inset (dashed lines with the grey axes).

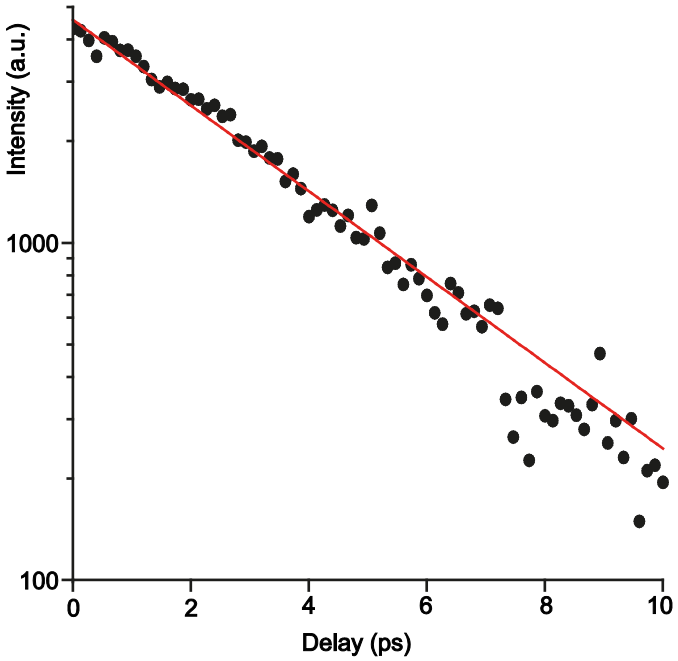


**Supplementary Figure 3. Transient transmission through the metamaterial.** Example of the time dependence of the transmitted light intensity of the cross-polarized component at a wavelength of 700 nm after the excitation shown in Fig. 2b from which decay constants are determined (3.4 ps with an error of 5%).

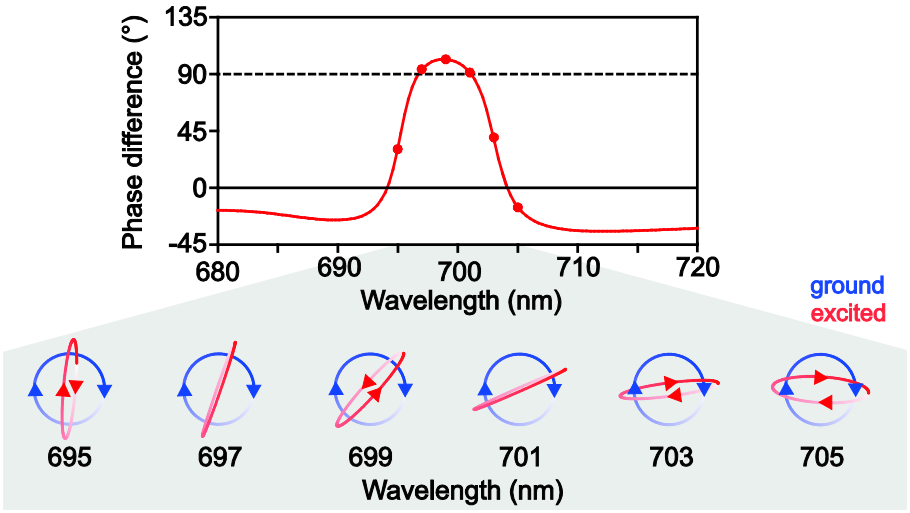


**Supplementary Figure 4. Simulated polarization handedness switching due to induced phase difference. (Top)** Change in relative phase between ordinary and extraordinary wave transmission coefficients upon control light illumination for the metamaterial as in Fig. 2. Dashed line indicates a phase difference of 90° which results in a conversion of circular polarization in the ground state to linear polarization in the excited state. **(Bottom)** the simulated excited (red) and ground (blue) state polarizations, with the ground state polarization chosen as right-hand circular. As the transmitted light wavelength crosses the resonance, a large change in phase occurs as shown in Fig. 1c. When traversing the resonance, the handedness of the transmitted light of the excited state transitions from right handed through linear to left handed whilst the ground state handedness remains constant. Going to longer wavelengths the excited state goes back to linear before becoming right handed once more.

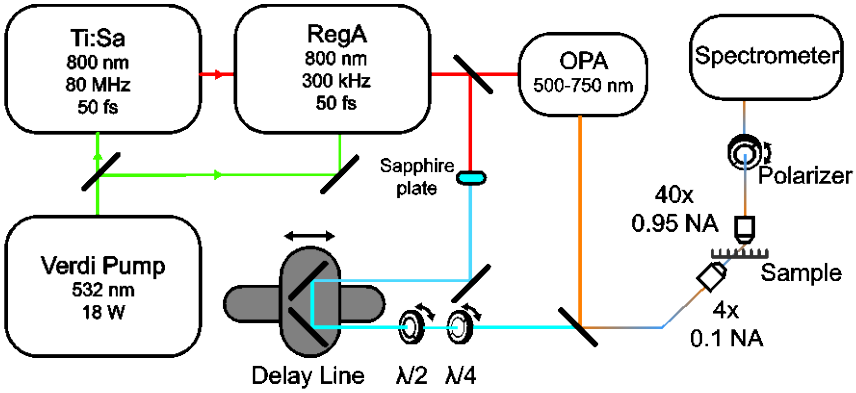


**Supplementary Figure 5. Experimental set-up.** Schematic of the time-resolved nonlinear polarization measurements.

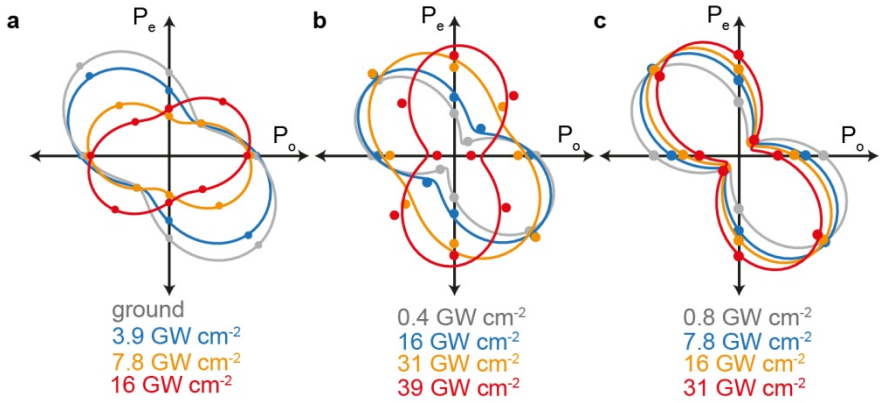


**Supplementary Figure 6. Fitting transmitted intensity for polarization retrieval.** Measured (symbols) and fitted (lines) intensity of the transmitted light at each analyzer angle used to recover the power dependent polarization changes in Fig. 4: **(a)** dependence of the polarization of the transmitted light at 700 nm on the intensity of the 585 nm control light, **(b, c)** the intensity dependence of the polarization ellipse rotation of the transmitted light on the on the intensity of the incident light for a wavelength **(b)** 700 nm for the metamaterial as in Fig. 2 with the *e*-wave resonance at 698 nm and **(c)** 600 nm for the metamaterial with *e*-wave resonance at 590 nm**.**